Dynamics and Kinetic Isotope Effect for the Double Proton Transfer in Formamidine Monohydrated Complex Using Direct Semiempirical Dynamics Calculation

Yongho Kim

Department of Chemistry and Institute of Natural Sciences, Kyung Hee University, Yongin-City, Kyunggi-Do, 449-701 Korea

Received: October 13, 1997; In Final Form: January 5, 1998

The dynamics of the double proton transfer in formamidine monohydrated complex has been studied by the direct semiempirical dynamics approach with variational transition-state theory using multidimensional semiclassical tunneling approximations. High-level ab initio quantum mechanical calculations were performed to estimate the energetics of the double proton transfer. Dimerization energies and the barrier height have been calculated at the G2* level of theory, which yields −7.50 and 16.6 kcal mol^{-1}, respectively. A quantum mechanical potential energy surface has been constructed using the AM1 Hamiltonian with specific reaction parameters (AM1-SRP) which are obtained by adjusting the standard AM1 parameters to reproduce the energetics by high-level ab initio quantum mechanical calculation. The minimum energy path has been calculated on this potential energy surface, and other characteristics of the surface were calculated as needed. The two protons are transferred synchronously, so the transition state possesses C_s symmetry. The reaction path curvature near the transition state is small, but that far from the transition state is large. Therefore the microcanonical optimized multidimensional tunneling approximation was used to calculate the tunneling coefficient. The tunneling amplitude initiated by reaction coordinate motion as well as that initiated by the vibrational mode normal to the reaction coordinate is important over the entire reaction coordinate. The distance that the proton hops during tunneling is about 0.62 Å at 300 K. This is a very long distance compared with the normal single proton transfer in solution. Before tunneling occurs, hydrogenic motion contributes minimally to the reaction path, which consists primarily of the heavy atoms moving to bring the formamidine and water molecules closer. This heavy-atom motion assists the tunneling process. The kinetic isotope effect (KIE) was also calculated. The quasi-classical contribution to the KIE is quite large due to the synchronous motion of the two protons. The tunneling contribution to the KIE determines the characteristics of the overall KIE in terms of temperature.

Introduction

Proton transfer has been studied extensively for a long time, since it is one of the simplest and the most fundamental reactions in chemistry and is important in oxidation−reduction reactions in many chemical and biological reactions.[1,2] Because of the light mass of the transferred atom, the importance of tunneling in proton-transfer reactions has been discussed for many years.[3] However multiproton transfers in which more than one proton is transferred, either synchronously or asynchronously, have not been extensively studied. Examples of multiproton transfer are proton relay systems in enzymes, proton transfers in DNA base pairs, certain proton transfers in hydrogen-bonded water complexes, and proton transfers in prototropic tautomerisms. Recently Limbach et al. have studied double proton transfer in prototropic tautomerisms for many formamidine systems and porphyrins using the dynamic NMR technique.[4−7] They reported rates and the kinetic isotope effects for both concerted[7,8] and stepwise[4−6] double proton transfer. Ernst et al. have studied double proton transfer in the crystalline benzoic acid dimer and measured the kinetic isotope effects.[9,10] They have suggested that tunneling has a predominant effect on the double proton transfer even at room temperature. Excited-state double proton transfers in which two protons are transferred cooperatively have been studied for hydrogen-bonded dimer, alcohol and water complexes of hydroxyquinolines, azaindoles, and other hydrogen-bonded systems.[11−24]

Recently many theoretical studies with ab initio quantum chemical methods at various levels have been carried out to predict the structures of the dimer and the potential energy surface for the various double proton transfer processes.[25−33] Scheiner et al. have studied and reviewed the potential energy surface for the proton transfer and the dimerization energy in a hydrogen-bonded system.[34,35] Hobza et al. have studied the potential energy surface (PES) for double proton transfer in the adenine−thymine base pair using various computational methods.[25−27] They have reported that the character of the PES, such as the barrier for the double proton transfer, strongly depends on the theoretical level of calculation: the size of the basis set and the inclusion of correlation energy.[27] However most of the earlier studies have focused on the geometrical change on dimerization and the energetic stabilization due to the hydrogen bonds in the dimer. Therefore the detailed dynamic features of the double proton transfer, such as tunneling and the effect of isotopic substitution, are not very well understood yet. To study the dynamics of such systems, one must know detailed information about the potential energy surface near the transition state and the critical configuration. Formic acid dimer (FAD) is one of most extensively studied systems both experimentally and theoretically,[36−41] and it is also

S1089-5639(97)03307-0 CCC: $15.00
Published on Web 04/07/1998

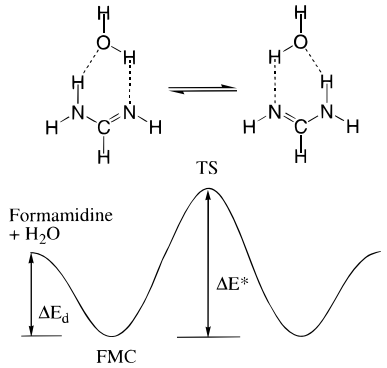

Figure 1. Schematic potential energy diagram for the double proton transfer in formamidine monohydrated complex.

one of the simplest examples of a multiproton transfer system in which the constituents are held together by two hydrogen bonds; so it can be used as a model of many chemically and biologically important multiproton transfers. Recently, we have carried out a direct semiempirical dynamics study for FAD; this study showed that tunneling is very important and that the most probable tunneling path is very different from the MEP.[42]

Since most proton transfers occur in aqueous solution, one must consider the role of water molecules in the proton transfer.[43] Water can act not only as a solvent but also as a mediator which gives or accepts protons to promote the long-range proton transfer. Jang and co-workers have reported that tunneling is very important in the water-mediated stepwise multiproton transfer of 7-hydroxyquinoline in aqueous solution.[44] Liedl et al. have studied concerted proton transfer in a cyclic water cluster using variational transition state theory with interpolated correction and including a semiclassical tunneling approximation, and they found that tunneling is significant in this reaction too.[45] Recently monohydrated formamidine has been studied by several researchers,[46−49] since amidine molecules have many biological and pharmaceutical uses.[50] Monohydrated formamidine is also one of the simplest examples for the water-mediated double proton transfer. The barrier for the prototropic tautomerization in this system is reduced by about 20 kcal mol^{-1} when the proton transfer is mediated by a water molecule.[46,47,49] Truong et al.[48] have carried out a direct ab initio dynamics study for the double proton transfer in monohydrated formamidine, and they showed that two protons are transferred synchronously, a water molecule reduces significantly the barrier for the prototropic tautomerization, and the tunneling effect is unusually large. However they have used the small-curvature semiclassical adiabatic ground-state tunneling approximation to calculate the tunneling probability. Since protons are transferred between nitrogen and oxygen atoms, this reaction corresponds to the heavy−light−heavy mass combination; therefore the large-curvature tunneling approximation may be more appropriate.[51] In this study, we have studied the double proton transfer in the formamidine monohydrated complex (FMC) using direct semiempirical dynamics calculations including the small-curvature, large-curvature, and microcanonical optimized multidimensional tunneling approximations. The kinetic isotope effects have also been calculated. We have compared the calculated rates and tunneling probabilities using the small-curvature approximation with those from the more complete direct ab initio dynamics calculation.

Figure 1 shows a schematic one-dimensional potential energy diagram for the double proton transfer in the FMC. A single transition-state structure with C_s symmetry is obtained in many calculations, which suggests that the double proton transfer in the FMC has a single transition state and proceeds through a concerted mechanism.[46−49] The dimerization energies, ΔE_d, and the potential energy barrier, ΔE^*, have been calculated using many different levels of quantum mechanical electronic structure theory, and the values of ΔE_d and ΔE^* vary significantly with the level of the quantum mechanical calculations.[46−49] In the present study, the G2* level of quantum mechanical calculation has been used to estimate ΔE_d and ΔE^*. In G2* theory, polarization functions on hydrogen were added to the standard G2 level basis sets.[52,53] The semiempirical molecular orbital method at the NDDO level, such as used in the AM1 or PM3 general parametrizations,[54] was used with specific reaction parameters[55] (SRP) to calculate the minimum energy path and the potential energy along it. The standard NDDO parameters were adjusted to reproduce the experimental dimerization energy and the theoretical potential energy barrier height determined by the G2* level calculations. Direct dynamics calculations have been carried out for the double proton transfer by variational transition state theory including tunneling contributions by multidimensional semiclassical approximations. The AM1 Hamiltonian was used as a starting point for the SRP adjustments, since it reproduces the dimerization energy and the structure of FMC better than the PM3. However the AM1 method produced an unreasonably large barrier height for the double proton transfer. So the standard AM1 parameters were modified to reproduce the values of ΔE_d and ΔE^* from experiment and G2* calculations, respectively, and the geometries of the monomer, dimer, and the transition state. The modified parameters, called AM1-SRP, were used for the direct dynamic calculations.

Theory

Rate constants were calculated by variational transition state theory.[56−62] The transition state was located at the position on the minimum energy path (MEP) where the calculated rate is a minimum. The Born−Oppenheimer potential on the MEP is called $V_{MEP}(s)$, where s is the reaction coordinate parameter, and the canonical variational transition state theory rate constant is given by[60,63]

$$k^{CVT}(T) = \min_s k^{GT}(T,s)$$

$$= \sigma \frac{k_B T}{h} \frac{Q^{GT}(T,s_*^{CVT})}{Q^R} \exp[-V_{MEP}(s_*^{CVT})] \quad (1)$$

The superscript GT denotes generalized transition state theory; k_B is the Boltzman constant; h is Planck's constant; s_*^{CVT} is the value of s at which k^{GT} is minimized, that is, the location of the canonical variational transition state; σ is the symmetry factor; and Q^{GT} and Q^R are partition functions for the generalized transition state and reactants, respectively.

To include the tunneling effect, the calculated rate constant, $k^{CVT}(T)$, is multiplied by a transmission coefficient, $\kappa^{CVT/G}$.

$$k^{CVT/G}(T) = \kappa^{CVT/G}(T)\, k^{CVT}(T) \quad (2)$$

The transmission coefficient is defined as the ratio of the thermally averaged quantal ground-state transmission probability, $P^G(E)$, to the thermally averaged classical transmission probability for the effective potential along the reaction

coordinate that is implied by CVT theory, $P_C^{CVT/G}(E)$:[60,64]

$$\kappa^{CVT/G}(T) = \frac{\int_0^\infty P^G(E)\, e^{-E/k_BT}\, dE}{\int_0^\infty P_C^{CVT/G}(E)\, e^{-E/k_BT}\, dE} \quad (3)$$

Since the value of $P_C^{CVT/G}(E)$ is unity above the threshold energy of the CVT calculation and is zero below, this expression reduces to

$$\kappa^{CVT/G}(T) = \frac{1}{k_BT} e^{V_a^G(s_*^{CVT})/k_BT} \int_0^\infty P^G(E)\, e^{-E/k_BT}\, dE \quad (4a)$$

$$= \frac{1}{k_BT} \kappa^{CVT/CAG} \int_0^\infty [P^G(E)\, e^{V^{AG}/k_BT}] e^{-E/k_BT}\, dE \quad (4b)$$

where

$$\kappa^{CVT/CAG} = e^{[V_a^G(s_*^{CVT}) - V^{AG}]/k_BT} \quad (4c)$$

and where $V_a^G(s_*^{CVT})$ is the ground-state adiabatic barrier evaluated at the canonical variational transition state, and V^{AG} is defined by

$$V^{AG} = \max_s V_a^G(s) \quad (4d)$$

Several semiclassical tunneling approximations were used to calculate $P^G(E)$. When the reaction path curvature is negligible so that the tunneling path coincides with the MEP, the minimum energy path semiclassical adiabatic ground state (MEPSAG) method is appropriate.[64] If the reaction path is curved but the curvature is small, tunneling is assumed to occur on a path defined by the classical turning points on the concave side of the MEP. This is an example of corner-cutting tunneling. For a polyatomic system with small reaction path curvature, the centrifugal-dominant small-curvature semiclassical adiabatic ground state (CD-SCSAG) tunneling approximation is appropriate.[54] When the reaction path curvature is large, which is typical for a bimolecular light-atom transfer between two heavy atoms, the large-curvature ground-state approximation, version 3 (LCG3), is appropriate.[60,63,65] In the LCG3 method, tunneling amplitudes are evaluated along all possible straight-line tunneling paths with equal kinetic energy before and after tunneling.

$$T_0(E) = \int_{-\infty}^{s_0} \frac{T_{tun}(\tilde{s}_0) \sin \chi(\tilde{s}_0,\tilde{s}_1)}{V_R(E,\tilde{s}_0)\, \tau(\tilde{s}_0)}\, d\tilde{s}_0 \quad (5)$$

In this equation, the primitive tunneling amplitude, $T_{tun}(s_0)$, is weighted by the sine of the angle between the vector along the tunneling path and the gradient vector at s_0 along the reaction coordinate, by the classical probability density $ds_0/V_R(E,s_0)$ that is proportional to the time spent by the system between s_0 and $s_0+\delta s_0$, where $V_R(E,s_0)$ is the local speed along the reaction coordinate, and by the number of collisions per unit time with the vibrational turning point in the tunneling direction $1/\tau$, where τ is the vibrational period.[60,63,65] The tunneling amplitude takes into account tunneling initiated by the vibrational motion normal to the reaction coordinate. To ensure microscopic reversibility, the total tunneling amplitude is calculated by

$$T_{vib}(E) = T_0(E) + T_1(E) \quad (6)$$

where $T_1(E)$ is the amplitude along the outgoing trajectory in the product channel from s_1 to $+\infty$. If the tunneling path has a component parallel to the reaction coordinate, then tunneling is also initiated by the reaction coordinate motion. The amplitude for the tunneling initiated by the reaction coordinate motion is given by

$$T_{rc}(E) = \{[\cos \chi(s_0) + \cos \chi(s_1)]/2\} \exp[-\theta(s_0)] \quad (7)$$

where $\chi(s_0)$ is the angle between the vector along the tunneling path and the gradient vector at s_0 along the reaction coordinate, and $\theta(s_0)$ is the imaginary action integral along the tunneling path. The contribution from tunneling along the reaction coordinate motion usually does not make a large contribution when the reaction path curvature is large. The primitive semiclassical transmission probability is given by

$$P_{prim}^{LCG3}(E) = T_{vib}(E)^2 + T_{rc}(E)^2 \quad (8)$$

The uniform semiclassical transmission probability is calculated by[60,63,65]

$$P^{LCG3} = \begin{cases} \left(1 + \frac{1}{2}\{[P_{prim}^{LCG3}(V^{AG})]^{-1} - 1\}[P_{prim}^{LCG3}(V^{AG})]^{-1} P_{prim}^{LCG3}(E)\right) & E_0 < E < V^{AG} \\ \times \{1 + [P_{prim}^{LCG3}(E)]^{-1}\}^{-1}, & \\ 1 - P_{prim}^{LCG3}(2V^{AG} - E), & V^{AG} < E < 2V^{AG} - E_0 \\ 1, & 2V^{AG} - E_0 < E \end{cases} \quad (9)$$

The microcanonical optimized multidimensional tunneling (μOMT) approximation estimates the optimal transmission probability as the larger of the transmission probabilities evaluated by the CD-SCSAG and LCG3 methods at a given energy.[55] The MEPSAG, CD-SCSAG, and LCG3 methods are called "zero-curvature tunneling" (ZCT), "small-curvature tunneling" (SCT), and "large-curvature tunneling" (LCT), respectively. The detailed mathematical derivations and computational formulas have been discussed and reviewed elsewhere.[60,63−65]

Computational Method

All electronic structure calculations were done using the GAUSSIAN 94 quantum mechanical package.[66] Geometries for formamidine, formamidine monohydrated complex, and the transition state were optimized at the Hartree−Fock (HF) level of theory and second order Møller−Plesset (MP) level of theory using the 6-31G(d,p) basis set. Energies at the stationary points have also been calculated at the G2* level theory.[52,53] In the standard G2 method, MP2(full)/6-31G(d) is used for the optimization of the geometry and energy. In this study polarization functions on hydrogen were added because hydrogen bonding is important. So the G2 type of energies in this study will be called G2* energies. Using MP2(full)/6-31G(d,p) geometries, single-point calculations were completed at the MP4/6-311G(2df,p), MP4/6-311+G(d,p), MP4/6-311G(d,p), MP2/6-311+G(3df,2p), and QCISD(T)/6-311G(d,p) levels. The MP4/6-311G(d,p) level was used as a starting point, and corrections were made for diffuse functions on nonhydrogen atoms, $\Delta E(+)$,

$$\Delta E(+) = \text{MP4/6-311+G(d,p)} - \text{MP4/6-311G(d,p)} \quad (10)$$

higher polarization functions on nonhydrogen atoms, $\Delta E(2df)$,

$$\Delta E(2df) = \text{MP4/6-311G(2df,p)} - \text{MP4/6-311G(d,p)} \quad (11)$$

with additional corrections for nonadditivity, $\Delta E(+,2df)$,

$$\Delta E(+,2df) = [MP2/6\text{-}311+G(2df,p) - MP2/6\text{-}311+G(d,p)] - [MP2/6\text{-}311G(2df,p) - MP2/6\text{-}311G(d,p)] \quad (12)$$

basis set enhancement, $\Delta E(3df,2p)$,

$$\Delta E(3df,2p) = MP2/6\text{-}311+G(3df,2p) - MP2/6\text{-}311+G(2df,p) \quad (13)$$

correlation effects beyond fourth-order perturbation, $\Delta E(QCI)$,

$$\Delta E(QCI) = QCISD(T)/6\text{-}311G(d,p) - MP4/6\text{-}311G(d,p) \quad (14)$$

higher level correction, $\Delta E(HLC)$,

$$\Delta E(HLC) = -0.00019n_{\alpha} - 0.00481n_{\beta} \quad (15)$$

and the zero-point energy, ΔZPE.

The G2* energy includes all of these corrections:

$$E(G2^*) = MP4/6\text{-}311G(d,p) + \Delta E(+) + \Delta E(2df) + \Delta E(+,2df) + \Delta E(3df,2p) + \Delta E(QCI) + \Delta E(HLC) + \Delta ZPE \quad (16)$$

Direct dynamics calculations were performed using the MORATE program.[67a] Frequencies were calculated as needed from MOPAC implemented in the MORATE program. We have correlated normal modes with a method implemented in a new version of the program [67b] and checked that adiabatic and diabatic interpolation of frequencies give almost no change in the rate constants. The Page−McIver method[68] is employed to calculate the minimum energy path (MEP). The MEP is scaled to a reduced mass μ of 1 amu. To take the tunneling effect on the double proton transfer into account, the CD-SCSAG (SCT), LCG3 (LCT), and μOMT methods were used. In the LCG3 method, tunneling amplitudes are calculated from the vibrational ground state of the reactant to all accessible vibrationally excited states of the product. Rates were calculated by canonical variational transition state theory using eqs 1−4 above.

Results and Discussion

The energies to form formamidine monohydrated complex (FMC) from formamidine and a water molecule and the barrier heights from the FMC to the double proton transfer transition state were calculated at various levels of quantum mechanical electronic structure theory in the previous studies by several other groups, and the results are listed in Table 1. The results in Table 1 show that the computed dimerization energy and the barrier height are very sensitive to the basis set and the treatment of the electron correlation. In the potential energy surface for double proton transfer in formic acid dimer, the dimerization energy and the barrier height are also very sensitive to the choice of basis sets and the inclusion of electron correlation.[32,42] In the density functional theory calculation, the values from Becke's hybrid half-and-half exchange with the Lee−Yang−Parr correlation (BH&H-LYP) method agree very well with those from high-level ab initio calculations including electron correlation. To obtain energetic information about the double proton transfer that is accurate enough to be used for an effective potential for the direct dynamics calculation, the G2* level of calculation was used. The results of the G2* calculation are listed in Table 2. The formation energies for FMC are −7.50 and −10.22 kcal mol^{-1} with and without zero-point energy correction, respectively. The barrier heights are 16.59 and 20.49 kcal mol^{-1} with and without zero-point energy correction, respectively. The barrier height from the G2* calculation agrees very well with that from the BH&H-LYP level of density functional theory. These energies were used to adjust the semiempirical MO parameters.

TABLE 1: Dimerization Energies and Barrier Heights for the Double Proton Transfer in Monohydrated Formamidine[a]

computational level	ΔE_d (kcal mol^{-1})	$\Delta E^{\ddagger}$ (kcal mol^{-1})
HF/4-31G//STO-3G		21.56[b]
HF/6-311G(d,p)//6-31G(d)	−9.7(−12.4)	32.1(29.4)[c]
MP2/6-311G(d,p)//HF/6-31G(d)	−12.8(−12.8)	23.6(20.9)[c]
MP4(SDTQ)/6-311G(d,p)// HF/6-31G(d)	−12.4(−15.1)	24.6(21.9)[c]
HF/6-31G(d,p)//6-31G(d)	−10.0(−12.7)	31.4(28.6)[c]
MP2/6-31G(d,p)//HF/6-31G(d)	−13.1(−15.8)	22.1(19.3)[c]
SAC2/6-31G(d,p)//HF/6-31G(d)		20.0(17.2)[c]
MP4(SDTQ)/6-31G(d,p)// HF/6-31G(d)	−12.7(−15.4)	23.5(20.7)[c]
HF/6-31G(d,p)		29.3(26.0)[d]
MP2/6-31G(d,p)		19.5(15.4)[d]
MP4(SDTQ)/6-31G(d,p)// MP2/6-31G(d,p)		21.4(17.3)[d]
CCSD(T)/6-31G(d,p)// MP2/6-31G(d,p)		21.9(17.8)[d]
BLYP/6-31G(d,p)		13.6[d]
BH&H-LYP/6-31G(d,p)		20.7(16.6)[d]
B3LYP/6-31G(d,p)		16.2[d]
G2*	−10.22(−7.50)	20.49(16.59)[e]

[a] The numbers in parentheses are with zero-point energies. [b] Reference 46. [c] Reference 47. [d] Reference 49. [e] This study.

The NDDO level of semiempirical MO calculation of the enthalpies of formation with standard AM1 parameters gives −59.27, −16.36, and −48.24 kcal mol^{-1} for H_2O, formamidine, and FMC, respectively, so the calculated enthalpy of dimerization is −5.33 kcal mol^{-1}. The calculated barrier height for the double proton transfer is 50.9 kcal mol^{-1}, which is very different from the corresponding G2* value. The structures of FMC and the transition state for the double proton transfer (FMCTS) from the AM1 calculations are also quite different from those of high-level ab initio calculations. The geometries for the FMC and the FMCTS, optimized at the MP2(full)/6-31G(d,p) level of theory and at the NDDO level of theory using standard AM1 parameters, are shown in Figures 2 and 3, respectively. In the optimized structure of FMC from the AM1 calculations, two protons in H_2O are weakly hydrogen-bonded to the nitrogen of imine in which the hydrogen bond lengths are 2.682 and 2.751 Å, as shown in Figure 2; however only one proton in H_2O is hydrogen-bonded from the MP2 level of ab initio calculations, and the hydrogen bond length is 1.931 Å. In the structure of FMCTS from the AM1 calculation, the protons on two N−H bonds are equally hydrogen-bonded to the oxygen in H_2O to form C_s symmetry, as shown in Figure 3, and the length of these hydrogen bonds is 1.666 Å. The bond length for the N−H bonds is 1.084 Å. These results mean that the transition state is a charge-separated ion-pair complex in which most of the positive charge is located on amidine group and the negative charge on oxygen. The reaction coordinate frequency at the FMCTS from the AM1 calculation is 826i cm^{-1}. However, in the structure of FMCTS from the MP2 calculation, the lengths for N−H and O−H bonds are 1.209 and 1.294 Å, respectively, and the reaction coordinate frequency is 1645i cm^{-1}. The geometries for FMC and FMCTS depend very much on the level of theory.

The standard AM1 parameters were adjusted, first, to reproduced the structures, frequencies, and the enthalpies of

TABLE 2: G2* Level Calculation for the Energetics of Double Proton Transfer in Formamidine Monohydrated Complex[a]

	FDW	FDWTS	FDM	H_2O
MP2/6-311G(d,p)	−225.905 094 6	−225.872 389 0	−149.620 376 2	−76.263 901 8
MP2/6-311+G(d,p)	−225.921 593 6	−225.889 703 6	−149.630 890 1	−76.274 714 1
MP2/6-311G(2df,p)	−226.016 765 6	−225.987 532 3	−149.695 520 5	−76.299 124 7
MP2/6-311+G(2df,p)	−226.031 234 6	−226.003 371 5	−149.704 947 6	−76.309 047 6
MP2/6-311+G(3df,2p)	−226.055 654 6	−226.026 029 6	−149.720 291 2	−76.318 268 3
MP4/6-311G(d,p)	−225.959 680 2	−225.924 780 3	−149.663 305 5	−76.276 279 4
MP4/6-311+G(d,p)	−225.976 366 8	−225.942 397 3	−149.673 786 8	−76.287 032 6
MP4/6-311G(2df,p)	−226.077 087 7	−226.045 451 8	−149.742 206 6	−76.313 603 1
QCISD(T)/6-311G(d,p)	−225.958 968 1	−225.923 328 1	−149.662 84	−76.276 277 4
$\Delta E(+)$	−0.016 686 6	−0.017 617 0	−0.010 481 3	−0.010 753 2
ΔE(2df)	−0.117 407 4	−0.120 671 5	−0.078 901 1	−0.037 323 7
$\Delta E(+,2df)$	0.002 030 0	0.001 475 4	0.001 086 8	0.000 889 4
ΔE(3df,2p)	−0.024 42	−0.022 658 1	−0.015 343 6	−0.009 220 7
ΔE(QCI)	0.000 712 0	0.001 452 2	0.000 465 5	0.000 002
ΔE(HLC)	−0.085	−0.085	−0.06	−0.025
ZPE[b]	0.081 882 4	0.075 664 6	0.056 749 2	0.020 804 5
E(G2*)	−226.118 569 8	−226.092 134 7	−149.769 73	−76.336 881 1
E(G2*)-ZPE	−226.200 452 2	−226.167 799 3	−149.826 479 2	−76.357 685 6

[a] The energies were calculated using the geometries optimized at the MP2(full)/6-31G(d,p) level of theory. Units in hartrees. [b] Zero-point energies were weighted by 0.95. [c] The barrier height for the double proton transfer is 16.59 kcal mol^{-1} including zero-point energy and 20.49 kcal mol^{-1} without zero-point energy. The formation energy for formamidine monohydrated complex is −7.50 kcal mol^{-1} including zero-point energy and −10.22 kcal mol^{-1} without zero-point energy.

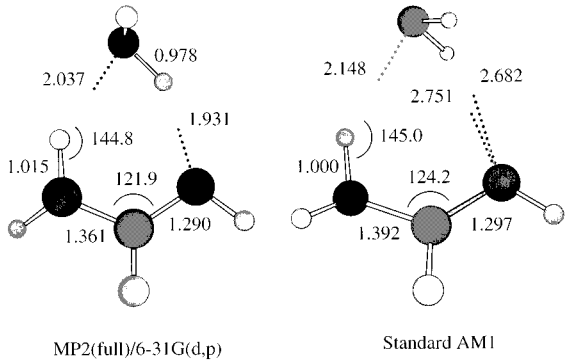

Figure 2. Geometries for the formamidine monohydrated complex optimized at the MP2(full)/6-31G** and the AM1 levels of theories. Lengths and angles are in angstroms and degrees, respectively.

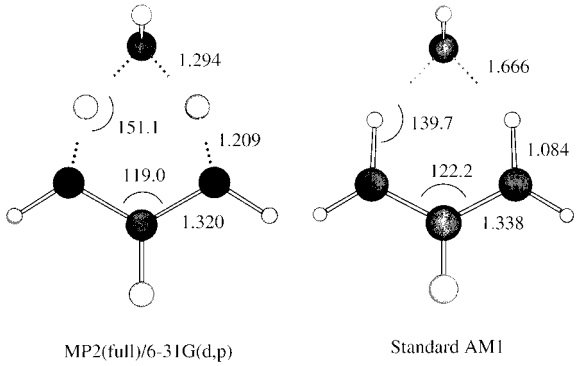

Figure 3. Geometries for the transition state for the double proton transfer in formamidine monohydrated complex optimized at the MP2-(full)/6-31G(d,p) and the AM1 levels of theories. Lengths and angles are in angstroms and degrees, respectively.

formation for formamidine and the FMC and, second, to reproduce the structure of the transition state, the barrier height, and the frequencies from the high-level ab initio calculation. We initially changed 45 parameters by hand (13 parameters each for C, N, and O, and 6 for H) and monitored the variation of energies and structures in terms of each parameter. Parameters that change the energies and structures were selected to reproduce the high-level ab initio calculation. Six parameters were chosen and adjusted further to reproduce the reaction

TABLE 3: Specific Reaction Parameters

atom	parameter[a]	AM1	AM1-SRP
H	ζ_s	1.188 078	1.002 000
H	α	2.882 324	3.282 324
N	β_p	−18.238 666	−17.238 666
N	α	2.947 286	3.047 286
O	α	4.455 371	4.555 371
O	G_{p2}	12.98	12.88

[a] ζ_s: slater exponent. α: core−core repulsion integral. β_p: resonance integral. G_{p2}: one-center electron repulsion integral.

coordinate frequency. The adjusted parameters are called specific reaction parameters (AM1-SRP),[55,69,70] and they are listed in Table 3. The absolute values of heats of formation for each species from the AM1-SRP method are different from those of the standard AM1 method. It was very difficult to get the specific reaction parameters that reproduce the structures, energies, and frequencies from the high-level ab initio calculations at the same time. However, in the dynamics calculation for the double proton transfer, the relative energies such as the barrier height and frequencies for the FMC and the FMCTS are most important. Therefore we paid more attention to reproduce these properties when we adjusted the AM1 parameters.

The optimized structures for FMC and FMCTS from the AM1-SRP method are shown in Figure 4. A proton in water is hydrogen-bonded in FMC, and the bond length is 1.821 Å. The bond lengths for N−H and O−H bonds in FMCTS are 1.202 and 1.305 Å, respectively. The geometries for FMC and FMCTS agree very well with those from the MP2(full)/6-31G-(d,p) method. The dimerization energy and the barrier height for the double proton transfer from the AM1-SRP method are −15.94 and 20.21 kcal mol^{-1}, respectively. The dimerization energy is slightly more negative compared with the G2* value, but the barrier height agrees very well with that from the G2* level of calculation. The frequencies for FMC and FMCTS from the MP2 and the AM1-SRP methods are listed in Table 4. The HF values of frequencies are generally about 10% overestimated, so they are scaled by 0.9. Electron correlation reduces the error in HF values to about 5%.[71] The frequencies calculated at the MP2 level were scaled by 0.95, but the AM1-SRP frequencies were not scaled. The AM1-SRP frequencies show fairly good agreement with those from the MP2(full)/6-31G(d,p) calculation.

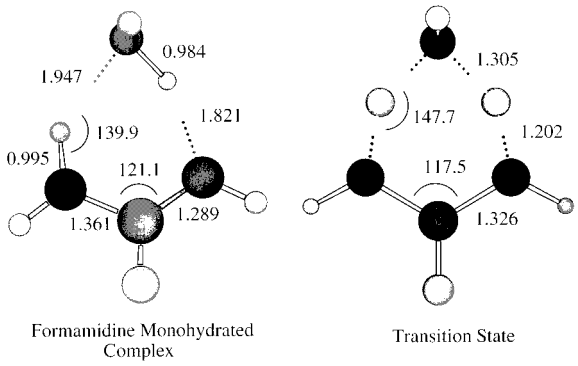

Figure 4. Geometries for the formamidine monohydrated complex and the transition state optimized at the AM1-SRP level of theory. Lengths and angles are in angstroms and degrees, respectively.

TABLE 4: Calculated Frequencies for FMC and FMCTS

FMCTS		FMC	
MP2(full)/ 6-31G(d,p)[a]	AM1-SRP	MP2(full)/ 6-31G(d,p)[a]	AM1-SRP
1563i	1574i	148	166
204	290	173	240
424	445	211	292
461	465	282	312
480	551	361	327
565	632	409	331
582	659	562	590
656	680	728	727
769	718	782	773
979	952	787	822
1055	1127	1016	957
1108	1149	1088	1073
1176	1220	1122	1162
1296	1254	1332	1250
1383	1285	1381	1501
1404	1369	1587	1600
1479	1586	1639	1639
1663	1611	1693	1902
1733	1825	3012	3082
1927	1846	3373	3083
3052	3113	3440	3302
3555	3521	3451	3459
3558	3528	3605	3537
3705	3574	3763	3500

[a] MP2 frequencies were weighted by 0.95.

The AM1-SRP imaginary frequency for the FMCTS also agrees very well with that from the MP2/6-31G(d,p) calculation. The imaginary frequency is determined by the shape of the potential energy surfaces along the reaction coordinate that is very important to the tunneling effect. This frequency calculated at the MP2 level is thought to be about 5% overestimated too, so it was scaled by 0.95.

Figure 5 shows the Born−Oppenheimer potential energy and the adiabatic ground-state potential energy along the MEP for the double proton transfer calculated from the AM1-SRP method. The adiabatic ground-state potential energy, V_a^G, is the sum of the Born−Oppenheimer potential (V_{MEP}) and the local zero-point energies. The shape of the barrier is almost symmetric, and the double proton transfer is a synchronous process. The transmission coefficients using the SCT, LCT, and μOMT approximations, denoted as κ_{HH}^{SCT}, κ_{HH}^{LCT}, and $\kappa_{HH}^{\mu OMT}$, respectively, and rate constants for double proton transfer with and without tunneling, calculated in the temperature range 150−500 K, are listed in Table 5. Bell and Truong[48a] have studied direct ab initio dynamics calculation for the same reaction. They followed a downhill gradient from the top of the barrier to obtain the MEP using the MP2/6-31G(d,p) level of theory, and they scaled the MP2 energies by a factor of 1.123 to match the CCSD(T)//MP2 barrier height, so their reaction coordinate might be narrower than what it should be, which generates larger tunneling probabilities. The results from the direct ab initio dynamics calculations are also listed in Table 5. The barrier height in this study is slightly larger than that of the direct ab initio dynamics studies, therefore, the quasiclassical rate constants without tunneling contribution are slightly smaller. The values of κ_{HH}^{SCT} and κ_{HH}^{SCT} are smaller too. These are reasonable since the imaginary frequency at the transition state is smaller than that from the direct ab initio dynamics study. Transmission coefficients and the rate constants using the LCT and the μOMT approximations are also listed. The κ_{HH}^{LCT} values are larger than the κ_{HH}^{SCT} values at temperatures below 300 K; however they are smaller above 300 K. The $\kappa_{HH}^{\mu OMT}$ values are closer to κ_{HH}^{LCT} values below 300 K, but closer to the κ_{HH}^{SCT} values above 300 K. In general, the representative tunneling path (RTP), where the thermally weighted transmission probability has a maximum, is close to the top of the barrier at higher temperature, and it is further from the top at low temperature, since tunneling becomes more important at low temperature. Therefore the fact that the κ_{HH}^{SCT} values are larger than the κ_{HH}^{LCT} values at the higher temperature suggests that the reaction path curvature of the potential energy surface is small near the top of the barrier. The reaction path curvature further down from the top of the barrier is larger, so the κ_{HH}^{LCT} value is larger at low temperature. Figure 6 shows the ground-state transmission probabilities, $P^G(E)$, calculated by the SCT and the LCT approximations as a function of V_a^G at the reaction coordinate turning point. The $P^G(E)$ values from the SCT approximation are larger than those from the LCT approximation at energies above 58.5 kcal mol^{-1} and are smaller below 58.5 kcal mol^{-1}. This means that the reaction path curvature of the potential energy surface may be considered small at energies above 58.5 kcal mol^{-1}, but should be treated as large below 58.5 kcal mol^{-1}. The thermally weighted $P^G(E)$ from the SCT and the LCT approximations at 200, 300, and 400 K are shown as a function of $V^{AG} - E$ in Figure 7, where, as defined in eq 4d, V^{AG} is the top of the adiabatic barrier. In this figure, the thermally weighted $P^G(E)$ is scaled by $\exp(V^{AG}/RT)$. The integral of these values divided by k_BT over energies gives the transmission probability, as shown in eq 4b. Since the relative size of the thermally weighted $P^G(E)$ from the SCT and LCT

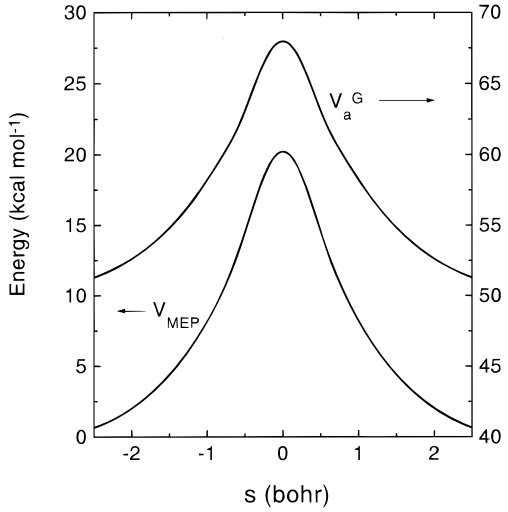

Figure 5. Classical and the adiabatic potential energy for the double proton transfer along the minimum energy path.

TABLE 5: Calculated Rate Constants and Transmission Coefficients in Double Proton Transfer[a]

T	k(HH)	κ_{HH}^{SCT}	κ_{HH}^{LCT}	$\kappa_{HH}^{\mu OMT}$	k_{HH}^{SCT}	k_{HH}^{LCT}	$k_{HH}^{\mu OMT}$
150	2.79×10^{-13} (4.29×10^{-11})	5.68×10^{9} (1.91×10^{9})	2.13×10^{11}	2.13×10^{11}	1.59×10^{-3} (8.18×10^{-2})	5.94×10^{-2}	5.94×10^{-2}
175	9.62×10^{-10}	1.41×10^{7}	2.73×10^{8}	2.74×10^{8}	1.35×10^{-2}	2.63×10^{-1}	2.63×10^{-1}
200	4.23×10^{-7} (1.77×10^{-5})	2.25×10^{5} (2.53×10^{5})	2.46×10^{6}	2.48×10^{6}	9.52×10^{-2} (4.48)	1.04	1.05
225	4.73×10^{-5}	1.17×10^{4}	7.54×10^{4}	7.77×10^{4}	5.51×10^{-1}	3.56	3.67
250	2.03×10^{-3} (3.94×10^{-2})	1.33×10^{3} (2.72×10^{3})	5.19×10^{3}	5.61×10^{3}	2.70 (107)	10.5	11.4
300	5.55×10^{-1} (6.51)	80.9 (200)	123	160	44.9 (1.30×10^{3})	68.0	88.8
350	29.9 (246)	17.3 (41.5)	14.2	22.2	517 (1.02×10^{4})	424	662
400	585 (3.7×10^{3})	7.25 (15.4)	5.09	7.86	4.24×10^{3} (5.71×10^{4})	2.98×10^{3}	4.60×10^{3}
500	3.71×10^{4} (1.63×10^{5})	3.08 (5.23)	2.38	3.12	1.15×10^{5} (8.52×10^{5})	8.85×10^{4}	1.16×10^{5}

[a] Numbers in parentheses are from the direct ab initio dynamics study.[48a]

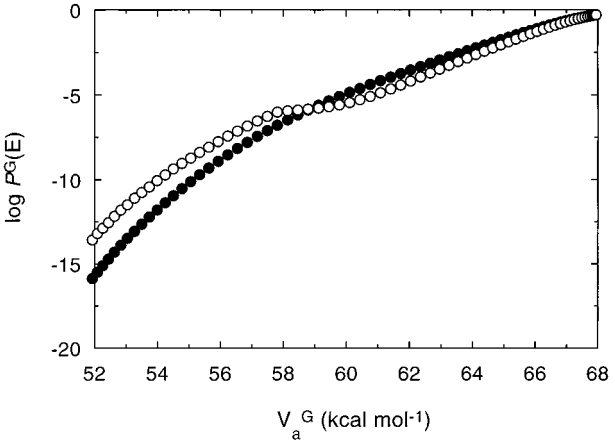

Figure 6. Transmission probability for the double proton transfer as a function of the adiabatic energy at the reaction coordinate turning point. The open and fill circles are for the values from the LCT and SCT approximations, respectively. Note that V_a^G at the reaction-coordinate turning point is the same as the total energy E.

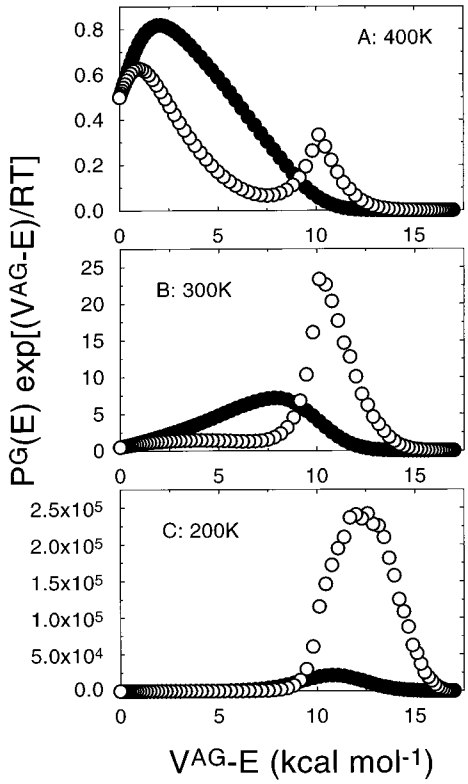

Figure 7. Thermally weighted transmission probability for the double proton transfer as a function of the $V^{AG} - E$ at various temperatures, where V^{AG} is the adiabatic energy barrier maximum (67.95 kcal mol^{-1}). The thermally weighted transmission probabilities are scaled by exp(V^{AG}/RT). Note that the $V^{AG} - E$ becomes larger as the total energy is reduced from the adiabatic energy barrier maximum.

methods varies with energy in such a way that neither one is always larger than the other, the μOMT approximation should be used to calculate the tunneling coefficients. At 200 K, the thermally weighted $P^G(E)$ from the LCT approximation are larger than those from the SCT approximation, and the energy at the RTP is 55.4 kcal mol^{-1}, which is about 12.6 kcal mol^{-1} below the top of the adiabatic energy barrier. The transmission coefficient is almost entirely determined by the transmission probabilities from the LCT method. However, at 400 K, the thermally weighted $P^G(E)$ from the SCT approximation are larger than those from the LCT approximation at energies above 58.5 kcal mol^{-1}, and the energy at the RTP is 65.9 kcal mol^{-1}, which is 2.0 kcal mol^{-1} below the top of the adiabatic energy barrier. The transmission coefficient is mostly determined by the transmission probabilities from the SCT method. At 300 K, the thermally weighted $P^G(E)$ from the SCT method are also larger at energies above 58.5 kcal mol^{-1}, but smaller than those from the LCT method below 58.5 kcal mol^{-1}. The transmission coefficient is determined by the tunneling probabilities from both the SCT and the LCT methods. The energy at the RTP is 57.7 kcal mol^{-1}, which is 10.3 kcal mol^{-1} below the top of the adiabatic energy barrier. The potential energy at the pretunneling configuration of RTP is 7.61 kcal mol^{-1}, which is 12.6 kcal mol^{-1} below the top of the potential energy barrier. The tunneling coefficients from the μOMT method increase rapidly with decreasing temperature, since the large curvature tunneling enhances the tunneling process at low temperature. The Arrhenius plots of calculated rates are shown in Figure 8. Tunneling noticeably enhances the rates, and the relative importance of small and large curvature tunneling approximations is changed at temperature between 300 and 350 K.

Figure 9 shows the lengths for the N−H and O−H bonds and the distance between O and C atoms along the minimum energy path. The RTP occurs from $s = -1.07$ to $s = 1.07$ at 300 K. From reactant to the pretunneling configuration on the RTP (from $s = -\infty$ to $s = -1.07$), the bond distances for the N−H and O−H bonds are rarely changed, but the distance between O and C is changed from 3.140 to 2.846 Å. The distance between O and C is 2.811 Å at the transition state;

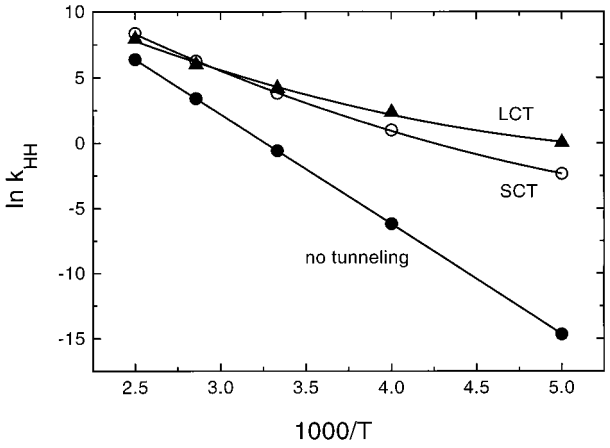

Figure 8. Arrhenius plot for the double proton transfer.

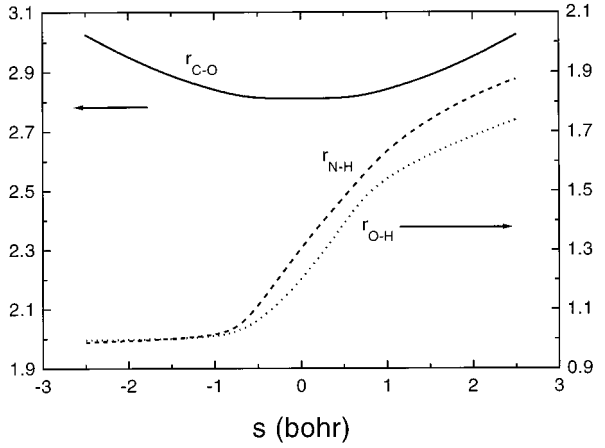

Figure 9. Bond distances in angstroms along the minimum energy path.

therefore about 90% of the change in this distance occurs before the RTP. The N−H and the O−H bond lengths are changed from 1.013 to 1.651 Å, and from 1.008 to 1.554 Å, respectively, between the pre- and posttunneling configurations; however the distance between O and N atoms is changed only 0.02 Å. Protons are moved about 0.62 Å by tunneling. Thus it is mostly heavy atoms that move when the reaction goes from the FMC up to the pretunneling configuration, and suddenly the two protons hop at that point. The N−H and the O−H bond lengths are continuously increased from the posttunneling configuration to the product (from $s = 1.07$ to $s = +\infty$), but in this case the protons in flight are already on the acceptor atoms, and the original bonds become the hydrogen bonds. These results are consistent with the previous studies for the double proton transfer in formic acid dimer.[42] At 400 K, the RTP occurs from $s = -0.3$ to $s = 0.3$, and the distance between O and C at the pretunneling configuration is 2.812 Å, which is almost the same as that at the transition state. The N−H and the O−H bond lengths are changed from 1.190 to 1.410 Å, and from 1.112 to 1.310 Å, respectively, between $s = -0.3$ and $s = 0.3$, so both protons are moved about 0.2 Å by tunneling. Truhlar and co-workers have reported direct dynamics calculations for the hydrogen atom transfer in the [1,5] sigmatropic rearrangement of *cis*-1,3-pentadiene, where the hydrogen atom moves about 0.2 Å by tunneling between two carbons at 470 K.[54] They have also studied the hydrogen-transfer reaction between CF_3 and CD_3H, where the hydrogen atom moves about 0.39 Å by tunneling but the C−C distance changes only 0.08 Å at 367.8 K.[55] However, the distances that two protons jump in FMC are larger than that for the typical single proton or hydride

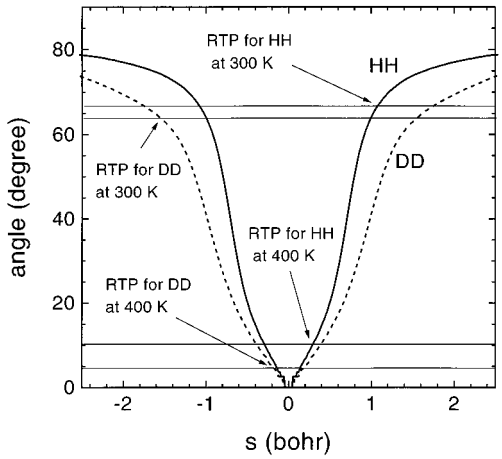

Figure 10. Angles between the LCG tunneling path and the reaction coordinate gradient vector at the classical turning point, *s*, along the minimum energy path.

transfer in solution. Consider, for example the potential energy surfaces for single hydride transfer between NAD^+ analogues in solution.[72] Analytical potential energy functions were fitted to reproduce experimental kinetic isotope effects for the hydride-transfer reactions. The RTP occurs about 1 kcal mol^{-1} below the top of the potential energy barrier, and the tunneling distance at the RTP for the hydride transfer between NAD^+ analogues is about 0.1 Å.[72] These results suggest that tunneling for the double proton transfer in the FMC is very efficient, and the RTP is very different from the MEP.

The angle between the MEP and a linear tunneling path from a pretunneling configuration to a posttunneling configuration is shown in Figure 10 for the double proton and the double deuterium transfers. At the transition state ($s = 0$), the angle is zero. As the reaction goes toward either reactant ($s = -\infty$) or product ($s = +\infty$), the angle for the double proton transfer increases slowly about 20° from $s = 0$ to $s = +0.5$ or -0.5. This indicates that the reaction path curvature is small near the transition state. This angle increases rapidly from 20° to 64° between $s = 0.5$ and $s = 1.0$ and increases slowly after $s = 1.0$. Along the reaction coordinates at $s < -1.0$, there is almost no hydrogenic motion as shown in Figure 9. Mostly heavy atoms move to bring water and formamidine molecules close together. Between $s = -0.5$ and $s = 0.5$, where the angle is small, there is almost no change in the distance r_{C-O}, but large change in the hydrogenic motion. The angles at the RTP are 10.3° and 66.4° at 400 and 300 K, respectively, for the double proton transfer. These are also shown in Figure 10. The RTP for the double proton transfer at 300 K is further from the transition state than that at 400 K, which is reasonable since tunneling is more important at lower temperature. At 400 K, since the angle at the RTP is small, the SCT approximation is appropriate, but at 300 K, the angle at the RTP becomes large; therefore the LCT approximation is appropriate. These results also suggested that the μOMT approximation, in which the transmission probability is the larger of the transmission probabilities evaluated by the LCT and the SCT approximations at a given energy, should be used to calculate the tunneling probability. The angles at the RTP for the double deuterium transfer are also shown in Figure 10, and they are 4.4° and 64.3° at 400 and 300 K, respectively.

The transmission coefficients and rate constants for the double deuterium transfer are listed in Table 6. The κ_{DD}^{SCT} values are larger than the κ_{DD}^{LCT} values at 300 K and above. The κ_{DD}^{LCT} values increase very rapidly with decreasing temperature. The

TABLE 6: Calculated Rate Constants and Transmission Coefficients in Double Deuterium Transfer

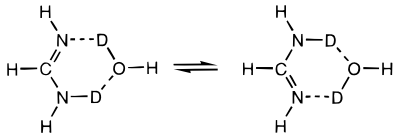

T	k(DD)	κ_{DD}^{SCT}	κ_{DD}^{LCT}	$\kappa_{DD}^{\mu OMT}$	k_{DD}^{SCT}	k_{DD}^{LCT}	$k_{DD}^{\mu OMT}$
150	4.24×10^{-15}	5.68×10^{7}	8.13×10^{9}	8.13×10^{9}	2.41×10^{-7}	3.45×10^{-5}	3.45×10^{-5}
175	2.59×10^{-11}	1.52×10^{5}	1.26×10^{7}	1.26×10^{7}	3.92×10^{-6}	3.26×10^{-4}	3.27×10^{-4}
200	1.74×10^{-8}	3.04×10^{3}	1.01×10^{5}	1.02×10^{5}	5.28×10^{-5}	1.75×10^{-3}	1.76×10^{-3}
225	2.69×10^{-6}	2.31×10^{2}	2.40×10^{3}	2.52×10^{3}	6.21×10^{-4}	6.46×10^{-3}	6.78×10^{-3}
250	1.49×10^{-4}	44.4	133	158	6.63×10^{-3}	1.98×10^{-2}	2.36×10^{-2}
300	6.02×10^{-2}	8.23	5.92	9.48	4.95×10^{-1}	3.56×10^{-1}	5.70×10^{-1}
350	4.27	3.93	2.82	3.98	16.8	12.0	17.0
400	103	2.65	2.10	2.66	274	217	275
500	8.90×10^{3}	1.79	1.57	1.79	1.59×10^{4}	1.39×10^{4}	1.59×10^{4}

TABLE 7: Calculated Double Deuterium Kinetic Isotope Effects and Tunneling Contribution to the Kinetic Isotope Effects

T	k(HH)/k(DD)	$\kappa_{HH}^{SCT}/\kappa_{DD}^{SCT}$	$\kappa_{HH}^{LCT}/\kappa_{DD}^{LCT}$	$\kappa_{HH}^{\mu OMT}/\kappa_{DD}^{\mu OMT}$	$k_{HH}^{SCT}/k_{DD}^{SCT}$	$k_{HH}^{LCT}/k_{DD}^{LCT}$	$k_{HH}^{\mu OMT}/k_{DD}^{\mu OMT}$
150	65.5	100	26.2	26.2	6598	1980	1980
175	37.1	92.8	21.7	21.7	3444	807	804
200	24.5	74.0	24.3	24.3	1803	595	596
225	17.6	50.6	31.4	30.8	887	551	541
250	13.5	30.0	39.0	35.5	407	529	483
300	9.20	9.83	20.8	16.9	90.7	191	156
350	6.99	4.40	5.04	5.58	30.8	33.4	39.0
400	5.63	2.74	2.42	2.96	15.5	12.8	16.7
500	4.16	1.72	1.52	1.74	7.23	6.37	7.30

$\kappa_{DD}^{\mu OMT}$ values are closer to κ_{DD}^{LCT} values at 250 K and below, but they are closer to the κ_{DD}^{SCT} values at 300 K and above. The relative importance of the SCT and the LCT tunneling probabilities switches at a temperature between 250 and 300 K. In the double proton transfer, the same change occurs at a temperature between 300 and 350 K. The calculated kinetic isotope effects (KIEs) at the various temperatures are listed in Table 7. The calculated KIEs at 300 K are very large, especially when one considers that the KIEs in single proton transfers are usually in the range 5−10, rising to about 20 in a few cases near room temperature.[2,3] Limbach et al. have determined the KIEs in other synchronous double proton transfers using the dynamic NMR method.[7,8] The KIE in the double proton transfer between acetic acid and methanol is 15 at 298 K,[8] and that in the substituted formamidine dimer is 237 at 189 K.[7] The calculated KIEs are also larger than those for the double proton transfer in formic acid dimer. The tunneling contribution to the KIE, κ_{HH}/κ_{DD}, is very large and it actually determines the characteristics of the total KIE. Bell and Truong[48b] have recently calculated the KIEs for the monodeuterated complex using the direct ab initio dynamics method, and they obtained 32.5 and 0.3 for $k_{HH}^{SCT}/k_{HD}^{SCT}$ and $(k_{HH}^{SCT}/k_{HD}^{SCT})/(k_{HD}^{SCT}/k_{DD}^{SCT})$, respectively, at 200 K. From these two values, one can obtain 3520 for $k_{HH}^{SCT}/k_{DD}^{SCT}$, which is 2 times larger than the corresponding value in this study. This is because the width of the barrier from the direct ab initio dynamics study is narrower than that in this study near the transition state. The KIEs from the LCT and the μOMT methods are smaller by a factor of 6 than the value of $k_{HH}^{SCT}/k_{DD}^{SCT}$ from the direct ab initio dynamics study. This is because the SCT method underestimates the tunneling probabilities for double deuterium transfer. The quasiclassical contribution to the KIE (KIE_{qc}) is 9.20 at 300 K, which is also large compared with the corresponding single proton transfer values. This is due to the synchronous hydrogenic motion of the two protons in flight, which raises the zero-point energy contribution to the KIE. If we take the rule of geometric mean,

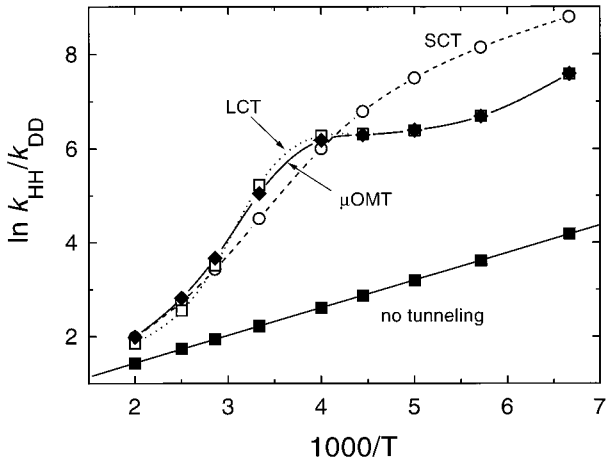

Figure 11. Plot of the KIEs vs inverse temperature with and without tunneling approximations.

the KIE_{qc} for each proton becomes 3.03 at 300 K, which is very reasonable.[2,3,72]

The values of KIEs increase with decreasing temperature. Figure 11 shows an Arrhenius plot for calculated KIEs with and without tunneling. The slope and intercept for the plot of ln KIE_{qc} vs $1/T$ are 588.6 and 0.255, respectively. From these values, the difference in the enthalpy of activation between the double proton and the double deuterium transfers is 1.17 kcal mol^{-1}, and that in the entropy of activation is 0.51 cal mol^{-1} K^{-1}. From these values, one can estimate that the enthalpic and entropic contributions to the KIE_{qc} are 7.12 and 1.29, respectively, at 300 K. The enthalpic contribution is very reasonable for the synchronous double proton transfer. The values of KIE_{qc} include contributions from the rotational and translational partition functions, in addition to those from the vibrational partition functions. The rotational and translational partition functions do not vary much with temperature, so the entropic contribution to KIE_{qc} is mainly due to the change in

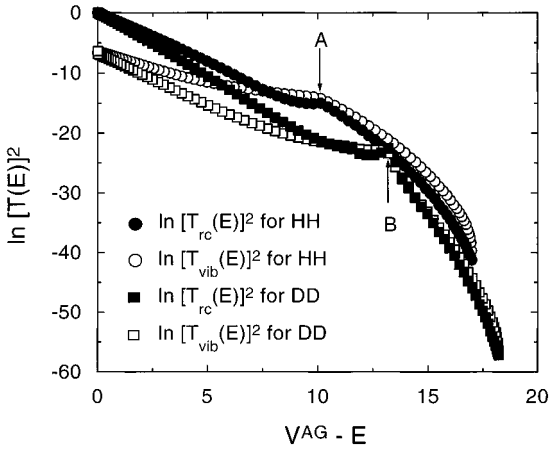

Figure 12. Tunneling amplitudes for the double proton and the double deuterium transfers as functions of energy. The larger values for $V^{AG} - E$ mean the further apart from the adiabatic barrier maximum. A and B are the energies of the RTP for the double proton and the double deuterium transfers at 200 K, respectively.

the vibrational partition functions. This suggests that the isotopically sensitive vibrational modes are coupled with various low-frequency vibrational modes.

Initially, the calculated KIEs with tunneling increase very rapidly with decreasing temperature. However the increasing rate is slowed down at very low temperature; therefore the overall shape of the Arrhenius plots of the calculated KIEs with tunneling is approximately sigmoidal. This behavior can be explained by the fact that the tunneling contributions for the double deuterium transfer as well as those for the double proton transfer increase with decreasing temperature, as shown in Tables 5 and 6. The κ_{HH}^{LCT} and κ_{DD}^{LCT} values both increase rapidly with decreasing temperature, but the increasing rates are different. In particular the values for κ_{DD}^{LCT} increase slowly at high temperature, but very rapidly at low temperatures, which produces the plateau on the plot of KIE vs reciprocal temperature. The RTP from the LCT method for the double proton transfer at low temperatures is very far from the transition state. The energy at the RTP for double proton transfer is 52.0 kcal mol^{-1} at 200 K, which is 13.2 kcal mol^{-1} below the top of the adiabatic energy barrier. This RTP occurs between $s = -1.57$ and $s = 1.57$ on the MEP, where there is almost no hydrogenic motion, and only heavy-atom motion which brings two molecules closer is important. The thermally weighted $P^G(E)$ for the double proton transfer behave quite similarly to those as shown in Figure 7c. Since the hydrogenic motion is minimal in this part of the potential energy surface, the reaction path curvature is not changed very much with the difference of the isotopic masses. Therefore the tunneling probability for the double deuterium transfer becomes closer to that of the double proton transfer at low temperature.

Figure 12 shows the tunneling amplitudes initiated by the reaction coordinate motion, $[T_{rc}(E)]^2$, and by the vibrational motion normal to the reaction coordinate, $[T_{vib}(E)]^2$, in terms of energy. The $[T_{rc}(E)]^2$ values are larger than the $[T_{vib}(E)]^2$ values near the transition state. This means that the LCG tunneling path has a large component parallel to the reaction coordinate, and the reaction path curvature is not large. This is consistent with the fact that the $P^G(E)$ values from the LCT method are smaller than those from the SCT methods near the transition state, as shown in Figure 9. When the reaction goes further down from the transition state, the $[T_{vib}(E)]^2$ values becomes larger than the $[T_{rc}(E)]^2$ values at energies below 60.4 kcal mol^{-1} (7.5 kcal mol^{-1} in terms of $V^{AG} - E$), but the difference is very small. These results are quite different from those for the double proton transfer in formic acid dimer, in which the $[T_{vib}(E)]^2$ values are several order of magnitude larger than the $[T_{rc}(E)]^2$ values over all the reaction coordinate, so the tunneling amplitude initiated by the reaction coordinate motion is not important to overall tunneling probability.[42] However in the FMC, the $[T_{rc}(E)]^2$ values are not negligible even at the potential surface, where the reaction path curvature is large. Truong and co-workers have reported that the dynamical coupling constants between the reaction path curvature and the eigenvectors for N−H and O−H stretching vibrational modes are fairly large.[48] These large dynamical coupling constants reduce the effective mass for the reaction to give eventually larger tunneling probability under the SCT approximation, and this may be considered to be our manifestation of vibrationally assisted tunneling (VAT). The reaction coordinate motion at the transition state is a synchronous motion which pulls one proton and pushes the other at the same time. This motion can be coupled with the O−H and N−H stretching vibrational motions. However the reaction coordinate motion far from the transition state, where the RTP occurs at low temperature, is mainly a heavy-atom motion which brings the two molecules together, as shown in Figure 9. Therefore the dynamical coupling constants for the O−H and N−H stretching modes become smaller, which means that the eigenvectors for these modes become closer to normal to the reaction coordinate vector, so the $[T_{vib}(E)]^2$ values become larger. The tunneling amplitudes for the double deuterium transfer behave quite similarly to those for the double proton transfer except that the energy where the $[T_{vib}(E)]^2$ values become larger than the $[T_{rc}(E)]^2$ values is lower. The tunneling amplitudes near the RTP at 200 K for the double deuterium transfer become close to those for the double proton transfer, as shown in Figure 12. This is consistent with the fact that the hydrogenic motion is minimal in this part of the potential energy surface, so the reaction path curvature is not changed very much with the difference of the isotopic masses. Figures 13 and 14 show the generalized frequencies along the reaction coordinates for the double proton and the double deuterium transfers, respectively. The N−H and O−H stretching modes are indicated, and the protons in N−H and O−H bonds are hydrogen-bonded to O and N, respectively. The RTP is represented as a vertical line. In Figure 13, the largest change in the vibrational frequencies is on the N−H and O−H stretching modes. The same is true in Figure 14.

The active N−H stretch, in Figure 13, has an avoided crossing with the C−H stretch at s about ± 1.2, which is very close to the RTP. This narrowly avoided crossing has not been observed in the direct ab initio dynamics study in which frequencies were calculated by the MP2 level of theory.[48a] So a reviewer was concerned about the possible error in the avoided crossing. We have correlated the frequencies using the REORDER option by calculating the overlap between vibrational modes from point to point on the MEP,[67b] but the avoided crossing remains the same. At $s = \pm 1.2$, the protons in flight are already transferred to the end atoms, as shown in Figure 9, so the N−H mode should be very close to that of the reactant and the product. The eigenvector for the N−H mode at the reactant has a small amount of the C−H stretching component, which makes an overlap between the N−H and the C−H modes and gives a narrowly avoided crossing. This small C−H stretching component exists in the N−H mode from the MP2 method too. The step size for the Hessian in the direct ab initio dynamics study was 0.1 bohr,[48a] which was too large to detect a narrowly

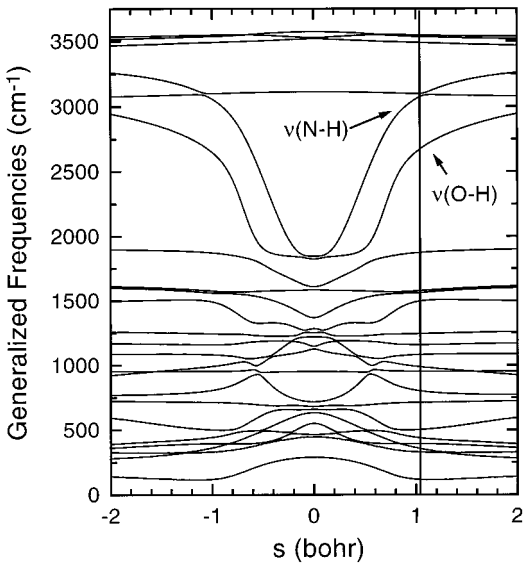

Figure 13. Generalized frequencies for the double proton transfer as functions of reaction coordinate. The vertical line is the point where the RTP occurs at 200 K.

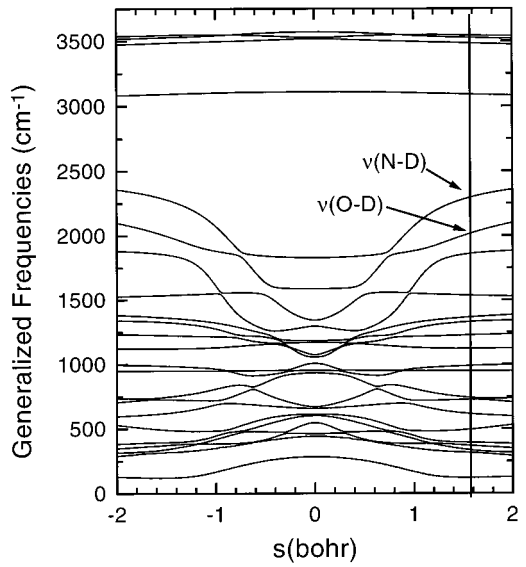

Figure 14. Similar to Figure 13, except for the double deuterium transfer.

avoided crossing. We increased our step size from 0.01 to 0.1 bohr, then the avoided crossing disappeared, and the transmission coefficients from the LCT method became 8%, 6%, and 1% smaller at 150, 300, and 500 K, respectively. These differences in the transmission coefficients are probably due to the small number of points that were used to calculate tunneling probabilities. The characteristics for the PES and the transmission coefficients in terms of temperature are all the same. These results suggest that the narrowly avoided crossing is not in error, and this does not affect the characteristics of the PES and the tunneling probabilities.

The curvatures for the $\ln[T(E)]^2$ plots are changed at the RTP, A and B in Figure 12. There is no unusual behavior in the frequencies near the RTP, as shown in Figures 13 and 14. Therefore the N−H and O−H stretching modes might be responsible for the curvature of the $\ln[T(E)]^2$ plots. Since the RTP depends on the temperature, the relative contribution of the $[T_{rc}(E)]^2$ and $[T_{vib}(E)]^2$ values to the tunneling probabilities changes with temperature. At 400 K the energy at the RTP is 65.9 kcal mol^{-1}, where the $[T_{rc}(E)]^2$ values are larger than the $[T_{vib}(E)]^2$ values, as shown in Figure 12; however the SCT method gives larger tunneling probability, as shown in Figure 7. Therefore the contribution from the $[T_{rc}(E)]^2$ and $[T_{vib}(E)]^2$ values to the tunneling coefficient is minimal. At 200 K the energy at the RTP is 55.5 kcal mol^{-1}, where $[T_{vib}(E)]^2$ values are slightly larger than the $[T_{rc}(E)]^2$ values. The tunneling coefficients are mostly calculated from the $[T_{rc}(E)]^2$ and $[T_{vib}(E)]^2$ values by the LCT method. At 300 K, as shown in Figure 7, the transmission probabilities from both the LCT and the SCT paths are important.

The tunneling amplitude initiated by reaction coordinate motion is reduced faster than that initiated by the vibrational motion normal to the reaction coordinate; however, these two amplitudes become quite close at the potential surface far from the transition state, and the difference is very small, as shown in Figure 12. This result means that the tunneling initiated by reaction coordinate motion is still important, and the motion in this part of the potential surface is mostly the heavy-atom motion to bring two molecules closer. Klinman and co-workers have reported kinetic isotope effects in enzyme reactions that are very large and almost independent of temperature.[73,74] These results may be explained if there is a large tunneling effect, possibly due to the VAT, and the RTP at the experimental temperature is so far from the transition state that the reaction path curvature is almost independent of the isotopic mass. The reaction coordinate motion that can assist tunneling in this case might be the protein motion.

Concluding Remarks

The double proton transfer reaction of the FMC has been studied with canonical variational transition state theory using multidimensional semiclassical tunneling approximations. The MEP was calculated by a direct semiempirical dynamics approach using the AM1-SRP method. The barrier height for the double proton transfer has been calculated with high-level ab initio calculations. From calculations at the G2* level the barrier height is estimated to be 20.49 kcal mol^{-1}.

The reaction path curvature varies considerably along the reaction coordinate, so the microcanonical optimized multidimensional tunneling (μOMT) approximation should be used. The tunneling amplitude initiated by reaction coordinate motion and that initiated by the vibrational mode normal to the reaction coordinate are both important over the whole reaction coordinate. The representative tunneling path (RTP) at 300 K occurs about 12.6 kcal mol^{-1} below the top of the potential energy barrier and is very different from the MEP. The distance that the proton hops from the N−H bond is 0.63 Å, and that from the O−H bond is 0.54 Å. These distances are very large compared with the tunneling distance in typical single proton transfers in solution. The kinetic isotope effect is also very large, and there is a plateau on the Arrhenius plot of the KIE. This can be explained by the VAT at the RTP far from the transition state, where the reaction path curvature is almost independent of the isotopic mass. The large quasi-classical contribution to the KIE is due to the synchronous hydrogenic motion of the two protons in flight.

Acknowledgment. We thank Professors M. M. Kreevoy and D. G. Truhlar, Department of Chemistry, University of Minnesota, for their helpful comments. We acknowledge the financial support from the SERI Supercomputer Center through the CRAY R&D Grant Program in 1997.

References and Notes

(1) Bender, M. L. *Mechanisms of Homogeneous Catalysis from Protons to Proteins*; John Wiley & Sons: New York, 1971; Chapters 2, 4, 5.

(2) Melander, L.; Saunders, W. H. J. *Reaction Rates of Isotopic Molecules*; John Wiley and Sons: New York, 1980; p 152.

(3) Bell, R. P. *The Tunnel Effect in Chemistry*; Chapman and Hall: New York, 1980.

(4) Schlabach, M.; Limbach, H.-H.; Bunnenberg, E.; Shu, A. Y. L.; Tolf, B.-R.; Djerassi, C. *J. Am. Chem. Soc.* **1993**, *115*, 4554.

(5) Scherer, G.; Limbach, H.-H. *J. Am. Chem. Soc.* **1994**, *116*, 1230.

(6) Scherer, G.; Limbach, H.-H. *J. Am. Chem. Soc.* **1989**, *111*, 5946.

(7) Meschede, L.; Limbach, H.-H. *J. Phy. Chem.* **1991**, *95*, 10267.

(8) Gerritzen, D.; Limbach, H.-H. *J. Am. Chem. Soc.* **1984**, *106*, 869.

(9) Meyer, R.; Ernst, R. R. *J. Chem. Phys.* **1990**, *93*, 5518.

(10) Stöckli, A.; Meier, B. H.; Kreis, R.; Meyer, R.; Ernst, R. R. *J. Chem. Phys.* **1990**, *93*, 1502.

(11) Negrerie, M.; Gai, F.; Lambry, J.-C.; Martin, J.-L.; Petrich, J. W. *J. Phys. Chem.* **1993**, *97*, 5046.

(12) Chen, Y.; Gai, F.; Petrich, J. W. *J. Am. Chem. Soc.* **1993**, *115*, 10158.

(13) Chen, Y.; Gai, F.; Petrich, J. W. *Chem. Phys. Lett.* **1994**, *222*, 329.

(14) Tokumura, K.; Watanabe, Y.; Itoh, M. *J. Phys. Chem.* **1986**, *90*, 2362.

(15) Chou, P.-T.; Martinez, M. L.; Cooper, W. C.; McMorrow, D.; Collins, S. T.; Kasha, M. *J. Phys. Chem.* **1992**, *96*, 5203.

(16) Chang, C.-P.; Hwang, W.-C.; Shin, M.-S.; Chou, P.-T.; Clements, J. H. *J. Phys. Chem.* **1994**, *98*, 8801.

(17) Fuke, K.; Yabe, T.; Chiba, N.; Kohida, T.; Kaya, K. *J. Phys. Chem.* **1986**, *90*, 2309.

(18) Chapman, C. F.; Maroncelli, M. *J. Phys. Chem.* **1992**, *96*, 8430.

(19) Moog, R.; Maroncelli, M. *J. Phys. Chem.* **1991**, *95*, 10359.

(20) Grabowska, A.; Borowicz, P.; Martire, D.; Braslavsky, S. E. *Chem. Phys. Lett.* **1991**, *185*, 206.

(21) Lee, S.-I.; Jang, D.-J. *J. Phys. Chem.* **1995**, *99*, 7537.

(22) Itoh, M.; Adachi, T.; Tokumura, K. *J. Am. Chem. Soc.* **1983**, *105*, 4828.

(23) Tokumura, K.; Itoh, M. *J. Phys. Chem.* **1984**, *88*, 3921.

(24) Baedez, E.; Boutin, P.; Valeur, B. *Chem. Phys. Lett.* **1992**, *191*, 142.

(25) Florián, J.; Hrouda, V.; Hobza, P. *J. Am. Chem. Soc.* **1994**, *116*, 1457.

(26) Hrouda, V.; Florián, J.; Hobza, P. *J. Phys. Chem.* **1993**, *97*, 1542.

(27) Hrouda, V.; Florián, J.; Polásek, M.; Hobza, P. *J. Phys. Chem.* **1994**, *98*, 4742.

(28) Tachibana, A.; Koizumi, M.; Tanaka, E.; Yamabe, T.; Fukui, K. *J. Mol. Struct.* **1989**, *200*, 207.

(29) Tachibana, A.; Ishizuka, N.; Yamabe, T. *J. Mol. Struct.* **1991**, *228*, 259.

(30) Topaler, M. S.; Mamaev, V. M.; Gluz, Y. B.; Minkin, V. I.; Simkin, B. Y. *J. Mol. Struct.* **1991**, *236*, 393.

(31) Agranat, I.; Riggs, N. V.; Radom, L. *J. Chem. Soc., Chem. Commun.* **1991**, *1991*, 80.

(32) Svensson, P.; Bergman, N.-Å.; Ahlberg, P. *J. Chem. Soc., Chem. Commun.* **1990**, *1990*, 82.

(33) Zielinski, T. J.; Poirier, R. A. *J. Comput. Chem.* **1984**, *5*, 466.

(34) Scheiner, S. In *Calculation the Properties of Hydrogen Bonds by ab Initio Methods*; Lipkowitz, K. B., Boyd, D. B., Eds.; VCH, New York, 1991; p 165.

(35) Scheiner, S. In *Proton Transfer in Hydrogen Bonded Systems*; Bountis, T., Ed.; Plenum: New York, 1992; p 29.

(36) Svensson, P.; Bergman, N.-Å.; Ahlberg, P. *J. Chem. Soc., Chem. Commun.* **1990**, *1990*, 862.

(37) Chang, Y.-T.; Yamaguchi, Y.; Miller, W. H.; Schafer, H. F., III. *J. Am. Chem. Soc.* **1987**, *109*, 7245.

(38) Shida, N.; Barbara, P. F.; Almlof, J. *J. Chem. Phys.* **1991**, *94*, 3633.

(39) Bertie, J. E.; Michaelian, K. H.; Eysel, H. H. *J. Chem. Phys.* **1986**, *85*, 4779.

(40) Bertie, J. E.; Michaelian, K. H. *J. Chem. Phys.* **1982**, *76*, 886.

(41) Millikan, R. C.; Pitzer, K. S. *J. Am. Chem. Soc.* **1958**, *80*, 3515.

(42) Kim, Y. *J. Am. Chem. Soc.* **1996**, *118*, 1522.

(43) Lim, J.-H.; Lee, E.-K.; Kim, Y. *J. Phys. Chem. A* **1997**, *101*, 2233.

(44) Kim, T.-G.; Lee, S.-I.; Jang, D.-J.; Kim, Y. *J. Phys. Chem.* **1995**, *99*, 12698.

(45) Liedl, K. R.; Sekusak, S.; Kroemer, R. T.; Rode, B. M. *J. Phys. Chem. A* **1997**, *101*, 4707.

(46) Yamabe, T.; Yamashita, K.; Kaminoyama, M.; Koizumi, M.; Tachibana, A.; Fukui, K. *J. Phys. Chem.* **1984**, *88*, 1459.

(47) Nguyen, K. A.; Gordon, M. S.; Truhlar, D. G. *J. Am. Chem. Soc.* **1991**, *113*, 1596.

(48) (a) Bell, R. L.; Truong, T. N. *J. Chem. Phys.* **1994**, *101*, 10442. (b) Bell, R. L.; Truong, T. N. *J. Phys. Chem. A* **1997**, *101*, 7802.

(49) Zhang, Q.; Bell, R.; Truong, T. N. *J. Phys. Chem.* **1995**, *99*, 592.

(50) Grant, R. J. In *The Chemistry of Amidines and Imidates*; Patai, S., Ed.; Wiley: New York, 1975; Chapter 6.

(51) Truhlar, D. G. *J. Chem. Soc., Faraday Trans.* **1994**, *90*, 1740.

(52) (a) Pople, J. A.; Head-Gordon, M.; Fox, D. J.; Raghavachari, K.; Curtiss, L. A. *J. Chem. Phys.* **1989**, *90*, 5652. (b) Curtiss, L. A.; Raghavachari, K.; Trucks, G. W.; Pople, J. A. *J. Chem. Phys.* **1991**, *94*, 7221.

(53) Curtiss, L. A.; Jones, C.; Trucks, G. W.; Raghavachari, K.; Pople, J. A. *J. Chem. Phys.* **1990**, *93*, 2537.

(54) Liu, Y.-P.; Lynch, G. C.; Truong, T. N.; Lu, D.-H.; Truhlar, D. G.; Garrett, B. C. *J. Am. Chem. Soc.* **1993**, *115*, 2408.

(55) Liu, Y.-P.; Lu, D.-h.; Gonzalez-Lafont, A.; Truhlar, D. G.; Garrett, B. C. *J. Am. Chem. Soc.* **1993**, *115*, 7806.

(56) Tucker, S. C.; Truhlar, D. G. In *New Theoretical Concepts for Understanding Organic Reactions*; Bertran, J., Csizmadia, I. G., Eds.; Kluwer: Dordrecht, Netherlands, 1989; pp 291−346.

(57) Truong, T. N. *J. Chem. Phys.* **1994**, *11*, 8014.

(58) Truhlar, D. G.; Garrett, B. C. *J. Chem. Phys.* **1979**, *70*, 1593.

(59) Truhlar, D. G.; Garrett, B. C. *J. Chim. Phys.* **1987**, *84*, 365.

(60) Truhlar, D. G.; Isaacson, A. D.; Garrett, B. C. In *Theory of Chemical Reaction Dynamics*; Baer, M., Ed.; CRC Press: Boca Raton, FL, 1985; p 65.

(61) Truhlar, D. G.; Garrett, B. C. *Annu. Rev. Phys. Chem.* **1984**, *35*, 159.

(62) Truhlar, D. G.; Isaacson, A. D.; Skodje, R. T.; Garrett, B. C. *J. Phys. Chem.* **1982**, *86*, 2252.

(63) Garrett, B. C.; Joseph, T.; Truong, T. N.; Truhlar, D. G. *Chem. Phys.* **1989**, *136*, 271.

(64) Garrett, B. C.; Truhlar, D. G.; Grev, R. S.; Magnuson, A. W. *J. Phys. Chem.* **1980**, *84*, 1730.

(65) Lu, D.-h.; Truong, T. N.; Melissas, V. S.; Lynch, G. C.; Liu, Y.-P.; Garrett, B. C.; Steckler, R.; Isaacson, A. D.; Rai, S. N.; Hancock, G. C.; Lauderdale, J. G.; Joseph, T.; Truhlar, D. G. *Comput. Phys. Commun.* **1992**, *71*, 235.

(66) Frisch, M. J.; Trucks, G. W.; Schlegel, H. B.; Gill, P. M. W.; Johnson, B. G.; Robb, M. A.; Cheeseman, J. R.; Keith, T. A.; Petersson, G. A.; Montgomery, J. A.; Raghavachari, K.; Al-Laham, M. A.; Zakrzewski, V. G.; Ortiz, J. V.; Foresman, J. B.; Cioslowski, J.; Stefanov, B. B.; Nanayakkara, A.; Challacombe, M.; Peng, C. Y.; Ayala, P. Y.; Chen, W.; Wong, M. W.; Andres, J. L.; Replogle, E. S.; Gomperts, R.; Martin, R. L.; Fox, D. J.; Binkley, J. S.; Defrees, D. J.; Baker, J.; Stewart, J. P.; Head-Gordon, M.; Gonzalez, C.; Pople, J. A. *Gaussian 94*; Gaussian, Inc.: Pittsburgh, 1995.

(67) (a) Hu, W.-P.; Lynch, G. C.; Liu, Y.-P.; Rossi, I.; Stewart, J. J. P.; Steckler, R.; Garrett, B. C.; Isaacson, A. D.; Lu, D.-h.; Melissas, V. S.; Truhlar, D. G. *MORATE-version 6.5*; University of Minnesota, Minneapolis, 1995. (b) Chuang, Y.-Y.; Hu, W.-P.; Lynch, G. C.; Liu, Y.-P.; Truhlar, D. G. *MORATE-version 7.2*; University of Minnesota, Minneapolis, 1997, based on *POLYRATE-version 7.2* by Steckler, R.; Chuang, Y.-Y.; Coitino, E. L.; Fast, P. L.; Corchado, J. C.; Hu, W.-P.; Liu, Y.-P.; Lynch, G. C.;Nguyen, K. A.; Jackels, C. F.; Gu, M. Z.; Rossi, I.; Clayton, S.; Melissas, V. S.; Garrett, B. C.; Isaacson, A. D.; Truhlar, D. G., University of Minnesota, Minneapolis, 1997, and *MOPAC-version 5.05mn* by Stewart, J. J.; Rossi, I.; Hu, W.-P.; Lynch, G. C.; Liu, Y.-P.; Truhlar, D. G., University of Minnesota, Minneapolis, 1995.

(68) Page, M.; McIver, J. W. *J. Chem. Phys.* **1988**, *88*, 922.

(69) Gonzalez-Lafont, A.; Truong, T. N.; Truhlar, D. G. *J. Phys. Chem.* **1991**, *95*, 4618.

(70) Rossi, I.; Truhlar, D. G. *Chem. Phys. Lett.* **1995**, *233*, 231.

(71) Bartlett, R. J.; Stanton, J. F. In *Applications of Post-Hartree-Fock Methods*; Lipkowitz, K. B., Boyd, D. B., Eds.; VCH, New York, 1994; p 65.

(72) Kim, Y.; Truhlar, D. G.; Kreevoy, M. M. *J. Am. Chem. Soc.* **1991**, *113*, 7837.

(73) Jonsson, T.; Glickman, M. H.; Sun, S.; Klinman, J. P. *J. Am. Chem. Soc.* **1996**, *118*, 10319.

(74) Glickman, M. H.; Wiseman, J. S.; Klinman, J. P. *J. Am. Chem. Soc.* **1994**, *116*, 793.